Dissecting a modified turbulent boundary layer using particle image velocimetry

Kevin[1], B. Nugroho[1], J.P. Monty[1] and N. Hutchins[1]

G. Pathikonda[2], J.M. Barros[2,3] and K.T. Christensen[2,4]

Corresponding author: kevin@student.unimelb.edu.au

[1] Dept. of Mechanical Engineering, University of Melbourne, Parkville, Vic 3053, Australia

[2] Dept. of Mechanical Science and Engineering, University of Illinois at Urbana-Champaign, Urbana, IL 61801, USA

[3] Dept. of Mechanical Engineering, United States Naval Academy, Annapolis, MD 21402, USA

[4] Dept. of Aerospace and Mechanical Engineering, University of Notre Dame, Notre Dame, IN 46556, USA

Abstract

Highly three dimensional turbulent boundary layers developed over herring-bone type riblet surface are investigated at moderate Reynolds number using particle image velocimetry (PIV) in all three orthogonal planes. Non-simultaneous measurements are performed to capture large fields of view (FOV) of more than 9δ in streamwise, 3δ in spanwise and 1.3δ in wall-normal direction in the respective planes. Observations of the instantaneous velocity fields reveal an extreme modification and rearrangement of the large-scale turbulence structures due to the unique surface topology. The utility of the multi-plane PIV diagnosis is that it uncovers structural modifications to the turbulent boundary layer that would have otherwise not been obvious from single point hot-wire anemometry. Distinct events observed in these multiple orientations are used to create a broader picture of this complicated flow. The new understanding of how turbulent boundary layers behave under the influence of three-dimensional secondary flow will be utilised to (re)tailor a passive surface for flow control purposes.

Introduction

The ability of herring-bone type riblets to impose large-scale secondary flow in turbulent boundary layers (without adding significant amount of parasitic form drag) was investigated by Nugroho *et al.* [7] using hot-wire anemometry. The motivation behind their research was to investigate the potential of this surface to manipulate large-scale coherent structures in wall-bounded turbulence. In their parametric study, they found a pronounced difference in the streamwise turbulence statistics between regions where the flow converges and diverges, despite the fact that those regions are only one boundary layer thickness apart in the spanwise direction. The local mean streamwise velocity decreases over the converging region (creating vertical flow away from the wall) and the local streamwise variance increases throughout the layer. This increase in velocity deficit results in the thickening of the local boundary layer (δ). Over the diverging region however, the opposite trend was observed. Furthermore, their analysis of the pre-multiplied energy spectra of the streamwise velocity fluctuation indicates an increase in the large-scale streamwise energy over the converging region with the opposite scenario over the diverging region. Without having spatial datasets, it was speculated that the surface might preferentially arrange or 'lock' the largest scale coherent structure over the converging region. In their further study, Nugroho *et al.* [8] mapped the mean cross-flow velocities over this herring-bone pattern using ×-wire probes. They mentioned that the combination of mean vertical flow away/towards the wall over the converging/diverging part of the riblets generates weak large-scale counter rotating roll-modes (with cross-flow terms of magnitude $\lesssim 2\%$ of freestream velocity U_∞ within their mea-

surement range). It is not immediately clear however, that these sluggish mean streamwise roll-modes are solely responsible for the substantial modifications to the boundary layer.

The aim of the current study is to investigate how the turbulence structures behave under this deliberately triggered secondary flow using instantaneous PIV flow fields. The large-field-of-view measurements were designed to capture the full-extent of the largest-scale modified structures.

Herring-bone type riblets

The riblet surface investigated in the present study was the same as that fabricated and studied by Nugroho *et al.* [8]. Figure 1(a) shows the key dimensional parameters of this surface roughness. The surface consists of repeating pattern of alternating converging and diverging grooves arranged in a 'herring-bone' like fashion. The height of each rib is $h = 0.5$ mm and the spacing is $s = 0.675$ mm, yielding $h^+ = hU_{\tau s}/\nu \approx 18$ and $s^+ = sU_{\tau s}/\nu \approx 24$ (where $U_{\tau s}$ is the smooth-wall friction velocity at the corresponding streamwise location and freestream velocity). Note that this tiny 'roughness element' has a blockage ratio of $h/\delta_s < 1\%$ (where δ_s is the corresponding smooth wall δ_{99} at the same inflow conditions). The ribs are yawed at an angle of $\gamma = \pm 20°$ from the main flow direction to create regions of convergence and divergence. The width of each converging/diverging region is 73.75 mm, giving a repeating spanwise wavelength of $\Lambda = 147.5$ mm. This converging-diverging wavelength corresponds to ~2.6 δ_s. Readers are referred to [7] for full details of the riblet manufacturing technique. To reduce background reflection in the PIV images, the riblet surface where the measurements were performed was dyed black using polymeric colourant.

PIV Experiments

Here x, y and z correspond to the streamwise, spanwise and wall-normal directions respectively, with u, v and w denoting the respective instantaneous velocity fluctuations.

Streamwise−wall-normal plane

Streamwise−wall-normal ($x - z$) planar PIV experiments were conducted in an open return blower wind tunnel of working section $6.7 \times 0.94 \times 0.375$ m^3 at the University of Melbourne. Full details of this wind tunnel can be found in Nugroho *et al.* [7]. The turbulent boundary layer was developed over the riblets for $X_r = 4$ m starting from the trip which is at the inflow to the working section. The flow was seeded with polyamide particles with mean diameter of 1 μm and illuminated using a dual cavity Big Sky Nd:YAG laser which delivers 120 mJ pulse^{-1}. The laser sheet was introduced from the downstream exit of the tunnel as shown in figure 1(b). Since the last optical compo-
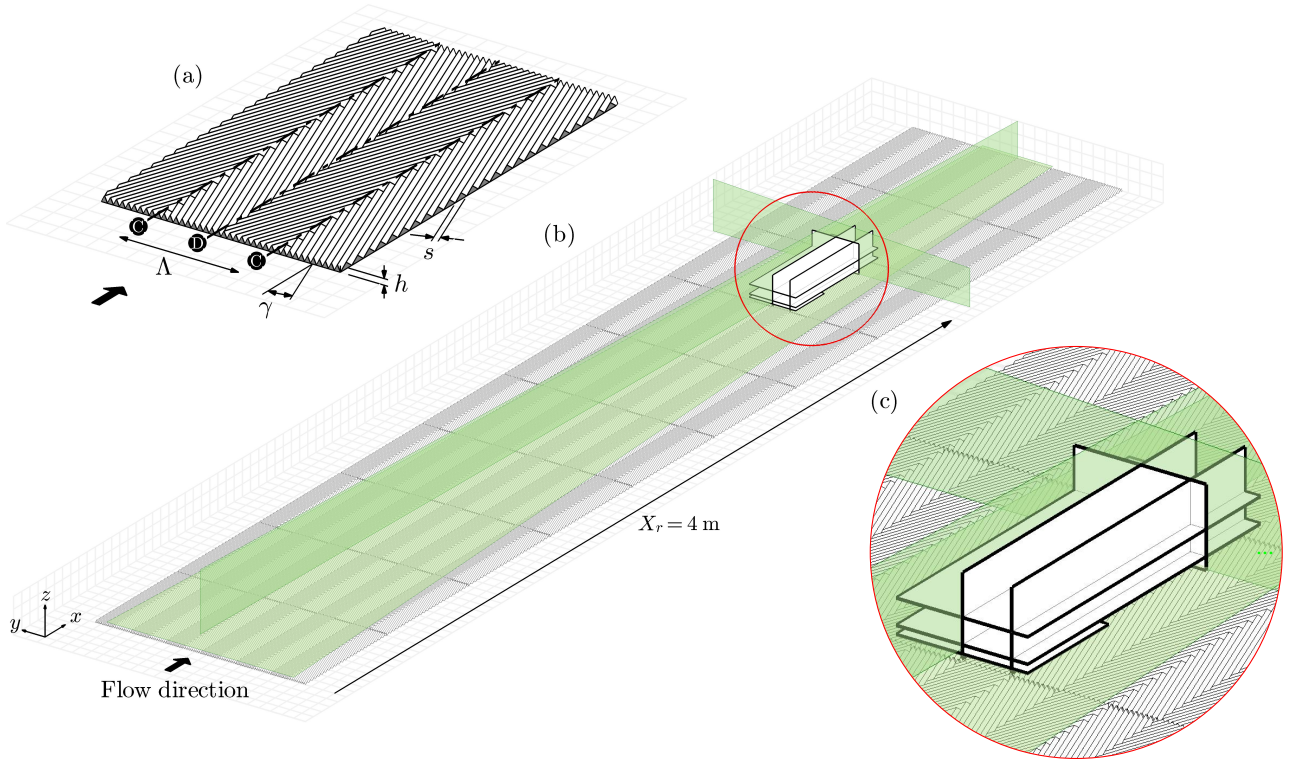
Figure 1: (a) Schematic diagram of the herring-bone riblets, showing the key surface parameters. Annotation **C** indicates the converging region and **D** the diverging region. (b) Schematic drawing of the PIV setup showing the measurement location and the direction of the laser sheets in the respective plane

Plane	Facility	U_∞ [m/s]	δ_s [mm]	δ_s^+	PIV config.	FOV $[\delta_s \times \delta_s]$	No. frames
$x-z$	Melbourne	15.2	56.7	2050	planar	9.1×2.3	3000
$x-y$	Melbourne	15.1	56.7	2050	planar	9.3×3.5	3000
$y-z$	Urbana-Champaign	17.0	96.2	3680	stereo	3.2×1.4	7000

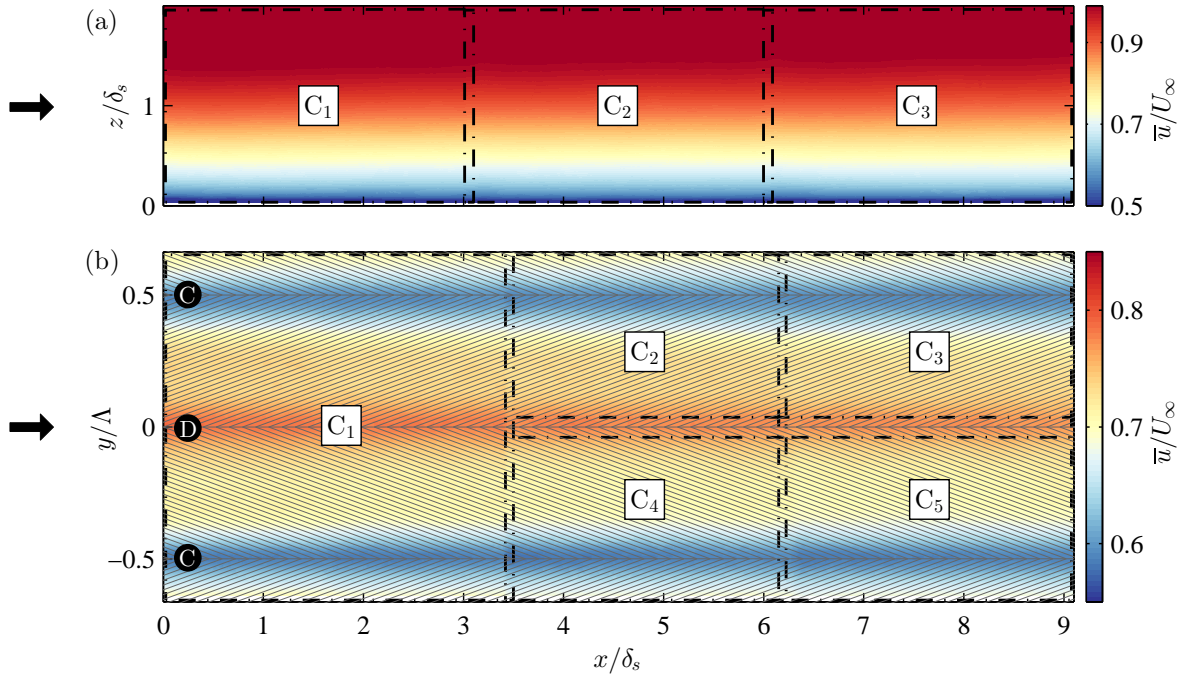Table 1: Summary of experimental parameters for the orthogonal-plane PIV experiments

Figure 2: Mean streamwise velocity fields normalised by the corresponding freestream velocity U/U_∞ across the FOV of the cameras; for (a) $x-z$ plane (over the converging region) and (b) $x-y$ plane. Dot-dashed lines indicate the extent of FOV per camera, and arrows indicate the flow direction
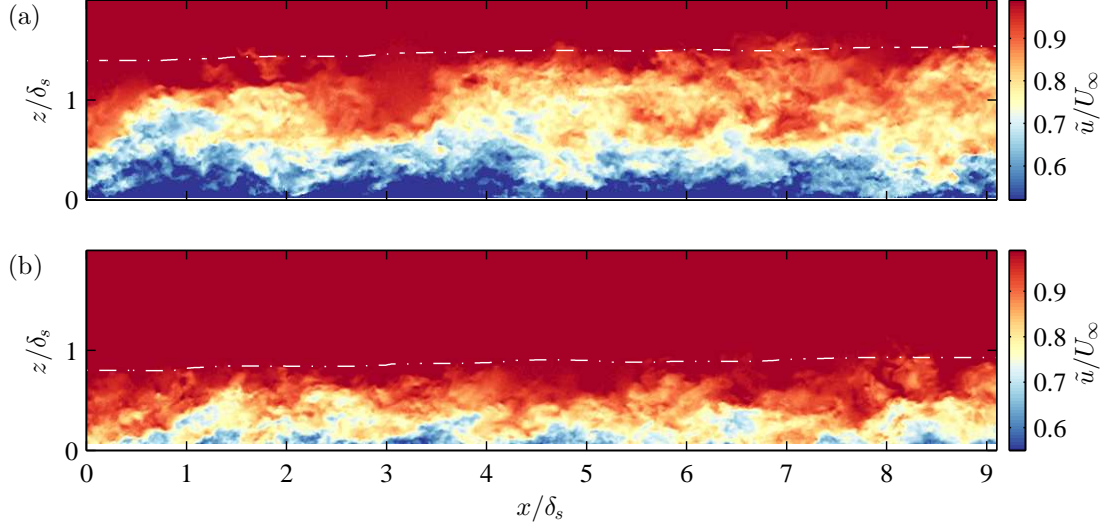
Figure 3: Representative instantaneous total streamwise velocity fields normalised by the freestream velocity $\tilde{u}/U_\infty$ over the (a) converging and (b) diverging part of the riblets. White dot-dashed line indicate the growth of local boundary layer thickness δ

nent is far away from the measurement location (over 3 m distance) with very minimal blockage, no effects were observed in the turbulence statistics. The illuminated flow was then imaged with three PCO4000 cameras (4008×2672 pixels, 14-bit frame-straddled CCD), equipped with Sigma 105mm macro lens. Figure 1(c) shows all the planes where the flow has been dissected. As indicated by the figure, the flow fields over the converging and diverging region were taken for the $x - z$ plane measurements. Figure 2(a) shows the mean streamwise velocity field over the converging part of the riblets. The figure indicates the extent of FOV captured by each camera. The overlap region between each camera FOV is at least 10 mm.

Wall-parallel plane

The streamwise-spanwise ($x - y$) plane experiments were also performed in Melbourne wind tunnel using planar configuration. Flow illumination technique, type of seeding and camera used are identical as the $x - z$ plane measurement. The wall-parallel views were obtained within the logarithmic region at $z = 6$ mm, in the outer layer at $z = 30$ mm and close to the wall at $z = 1.5$ mm. In both log and wake region measurements, five-camera configuration was employed. Figure 2(b) shows the mean streamwise velocity field from the log region measurement. The flow direction is from left to right. The riblets pattern is superimposed to indicate the converging/diverging region. Note that the number of lines drawn does not represent the actual number of ribs per converging-diverging wavelength Λ (more than 200 ribs to form Λ). Annotation **C** and **D** are also used to indicate the converging and diverging region respectively. The figure also highlights the extent of FOV captured by each camera. Camera C_1 was equipped with 60mm Nikon lens to get a bigger field of view, while C_{2-5} with Sigma 105mm lens. In the sublayer measurement however, the laser sheet was sent from the side of the tunnel and only two cameras (similar to C_2 & C_4 setup) were used.

Cross-flow plane

The cross-plane ($y - z$) view experiment was performed as a collaboration with the University of Illinois at Urbana-Champaign. The measurement was conducted in an open return suction-type wind tunnel with working section of $6 \times 0.914 \times 0.457$ m^3 (details of the tunnel can be found in Wu & Christensen [12]). Unlike the other plane measurements, here the turbulent boundary layer was first developed over a smooth wall for 1 m, then transitioned to the rough surface (the crest of the riblets is flush

with the upstream smooth wall) and developed over the riblets for 4 m. The flow was seeded with 1μm olive oil droplets generated using a Laskin nozzle and illuminated with a 1.5 mm thick laser sheet generated by a dual-cavity pulse Nd:YAG laser (Quantel). The imaging system is two TSI 11MP cameras (4000×2672 pixels, 12-bit frame-straddled CCD) equipped with Sigma 180mm macro lens. For this stereoscopic PIV configuration, the cameras viewed the cross-flow plane from both sides of the tunnel at upstream angle of $\pm 45°$ from the streamwise direction. Uniform image focus was obtained across the entire field of view by satisfying the Scheimpflug condition.

The particle images in all measurement planes were processed using an in-house PIV package. The details of the PIV processing algorithm are available in de Silva et al. [10]. For the stereoscopic dataset, three velocity components are reconstructed from the pixel displacements of the raw images based on the method proposed by Soloff et al. [11]. The extent of field of view and other PIV parameters in all measurement planes are summarised in table 1. Three thousand statistically independent velocity fields (per camera) were processed for each plane in the planar PIV measurements, and seven thousand for the stereoscopic measurement.

Velocity fields

To account for the spanwise heterogeneity over the riblets, the velocity components are decomposed into three components [1],

$$\begin{aligned}
\tilde{u}_i &= U_i(z) + \hat{u}_i(x,y,z) + u_i(x,y,z,t) \\
&= U_i(z) + u_i'(x,y,z,t) \\
&= \overline{u}_i(x,y,z) + u_i(x,y,z,t)
\end{aligned} \qquad (1)$$

where U_i is the spatially and temporally averaged mean velocity (global mean), and $\hat{u}_i = \overline{u}_i - U_i$ is the spatial variation of the time-averaged velocity. The term u_i is the turbulence fluctuation (convecting turbulence) about the time-averaged mean, and u_i' is the combination of both convecting and non-convecting fluctuations.

Streamwise−wall-normal plane

Figure 3 (a) and (b) show examples of instantaneous streamwise velocity field over the converging and diverging regions respectively. It must be noted that these flow fields were taken non-simultaneously (taken from separate experiments). However, in both cases all the flow conditions are the same. The
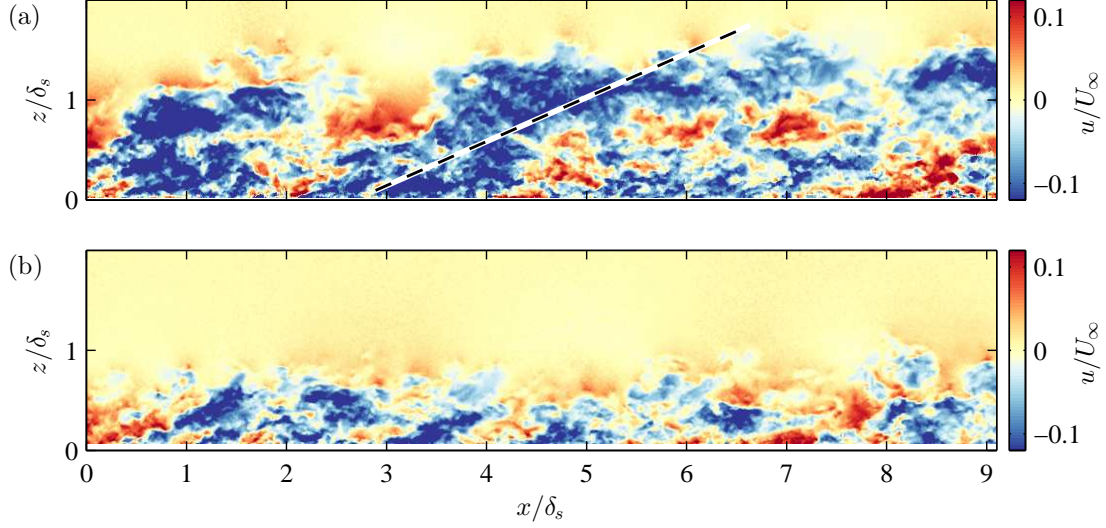
Figure 4: Representative instantaneous convecting streamwise velocity fluctuation normalised by the freestream velocity u/U_∞ over the (a) converging and (b) diverging part of the riblets. Dashed black lines indicate the inclination of the structure

flow direction is from left to right and the $\tilde{u}$ is normalised by the corresponding freestream velocity U_∞. Both abscissa and ordinate are normalised by the mean smooth-wall boundary layer thickness δ_s to highlight the modification caused by the surface roughness. Aligned with the previous observation by Nugroho *et al.* [7, 8], the boundary layer over the converging region seems to be thicker and exhibiting more intense turbulence activity. These phenomena (also accompanied by higher local friction velocity U_τ) result in higher local Reynolds number over the converging region. Over the diverging region however, the boundary layer is thinner with much lower turbulence intensity observed. It is fascinating that such different flow structures and turbulence level are consistently present with only $1\delta_s$ separation in the spanwise direction.

Figure 4 shows the convecting streamwise turbulence fluctuations u associated with figure 3. These representative examples clearly contrast the typical turbulent event that predominate over different regions of the riblets. Over the converging region, the large-scale low speed events which Kim & Adrian [3] suggest to be the agglomerations of hairpin packets, seem to be bigger instantaneously. They also often have the attributes that are uncommonly seen in the smooth-wall boundary layer, such as the inclination angle of the structure as indicated by the dashed line in figure 4 (a). Although not shown here for brevity, the ejections (wall-normal velocity component $\tilde{w}$) underneath these events can actually reach 20% of U_∞ (higher than $5U_{\tau s}$)for this example. Opposite trends are observed over the diverging region. The u fluctuations often seem to be more compact and at much lower amplitude (even compared to the smooth-wall case), which result in the reduced turbulence intensity as previously reported in [7]. It also appears that the events have an enhance periodicity in the streamwise direction.

Wall-parallel plane

It is important to note that all the streamwise-spanwise measurements presented here are 'true wall-parallel' views, i.e. the planes taken did not follow a constant normalised height such as constant z/δ or constant zU_τ/ν. The constant normalised height approached was not considered since both δ and U_τ are function of spanwise location. Furthermore, it was also found that the boundary layer thickness over the converging and diverging regions grow at slightly different rates within the streamwise domain captured. Figure 5 shows an example of total streamwise velocity field $\tilde{u}$ for three different wall heights. The streamwise axis is normalised using the smooth-wall boundary layer thickness δ_s but the spanwise axis using the converging-

diverging wavelength Λ (while maintaining the physical aspect ratio). Here the diverging region is located at $y/\Lambda = 0$ and converging region at $y/\Lambda = \pm 0.5$. The figure showcases the different appearance of the modified turbulent boundary layer at different wall distances.

Figure 5(a) is an example of streamwise velocity field taken at 1.5 mm above the crest of the riblets ($z = 3h$). Although at this height $zU_{\tau s}/\nu \approx 55$, the resemblance of the small-scale near-wall streakiness is still apparent. The wide spanwise periodicity can also be observed even at this height. The other feature that is commonly observed is the number of low-speed streaks collected around the converging region (highlighted by the inset). A time-resolved dataset would be desirable to explain the dynamics of this bunching of streaks.

Figure 5(b) is a representative flow field within the logarithmic region ($zU_{\tau s}/\nu \approx 220$). In canonical wall turbulence, the most prevalent feature in this layer is the very long coherent structures, termed 'superstructures' by Hutchins & Marusic [2]. These large scale features are known to have significantly meandering tendency, have distinct modulating influence on the small-scale signal near the wall (Mathis *et al.* [4]), and are present in other flow geometries such as channel and pipe (Monty *et al.* [5]). The instantaneous fields over the riblets however, show significant difference in the arrangement of the low and high momentum regions. Strong retarded features seem to always occupy the region over the converging part of the riblets as shown in figure 5(b). These strongly streamwise-aligned features seems to often extend longer than the field of view, and therefore appear strongly in the mean velocity field shown in figure 2(b). The best explanation so far regarding the formation of this infinitely long mode is that, at this height the secondary flow has gathered the near-wall streaks creating a 'superburst' of increased turbulent activity (refer to Na *et al.* [6] for 'superburst' discussion).

Figure 5(c) is a representative streamwise velocity field within the wake region, taken at 30 mm above the crest of the riblets ($z \approx 0.5\delta_s$). The fields at this height feature the growth in the spanwise width of these low momentum regions. An unexpected behaviour of these long streaks is also occurred. The streaks no longer seem so straight or well-aligned in the streamwise direction, showing signs of large-scale three-dimensional distortion and instability. It is speculated at this point that this event might correspond to the strong ejection described previously in the $x - z$ plane. Further analysis on the frequency and
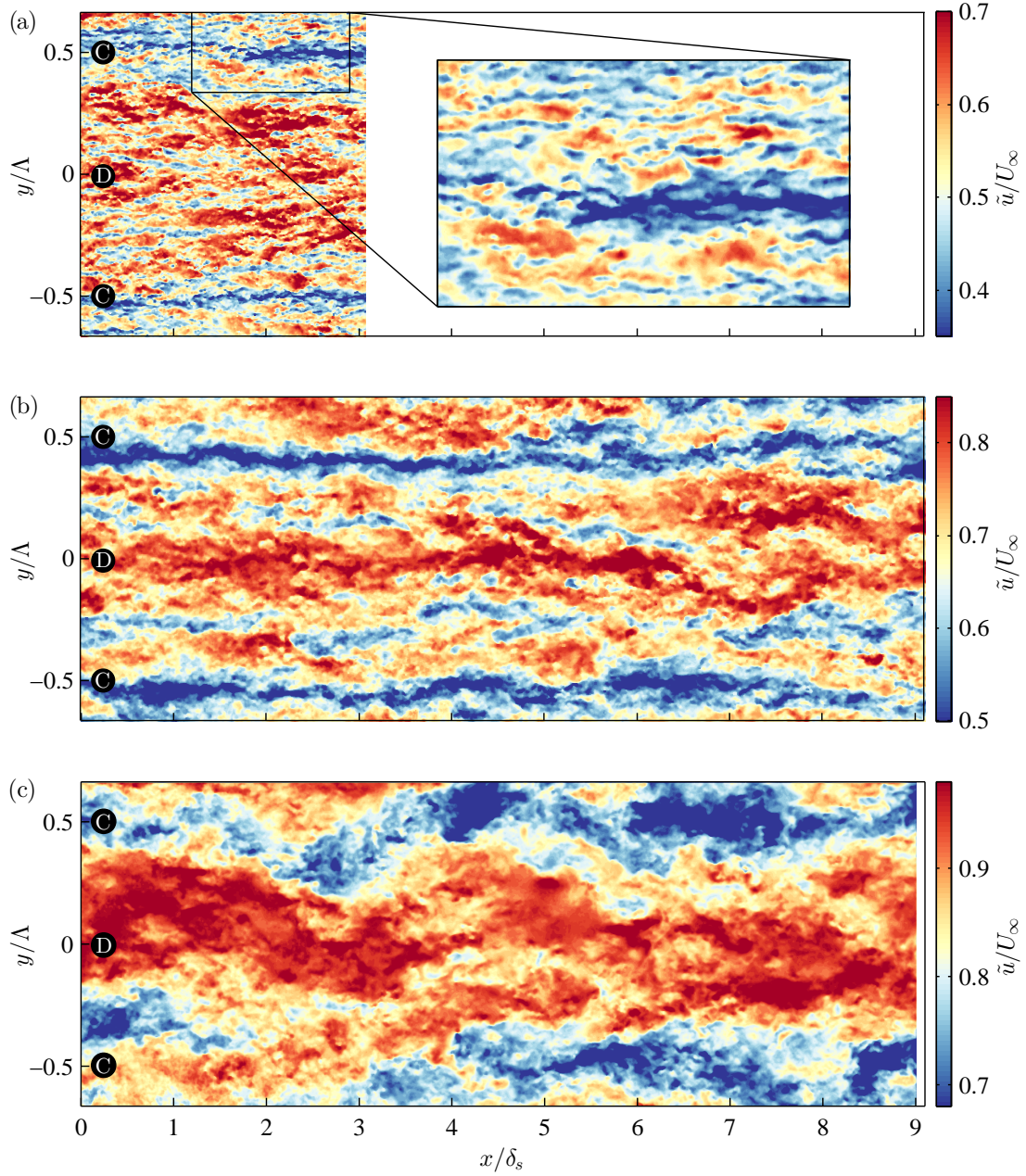
Figure 5: Example of instantaneous streamwise velocity fields in wall-parallel plane at three different layers. (a) within the roughness sublayer at $z = 1.5$ mm. (b) within the logarithmic region at $z = 6$ mm. (c) in the wake region at $z = 30$ mm.

dominant length scale of this event is required to confirm this argument. Although not shown here for brevity, spanwise velocity fields $\tilde{v}$ often exhibit wide regions of alternating positive and negative velocities in the streamwise direction at this z location.

Cross-flow plane

Figure 6 shows a typical streamwise velocity field over the riblets. The flow direction is out of the page. The spanwise axis is again normalised by the converging-diverging wavelength Λ and wall-normal axis by the corresponding δ_s. The spanwise periodicity in the local time-averaged boundary layer thickness δ is indicated by the dot-dashed line. It is important to note that the ratio Λ/δ is slightly different for the Urbana-Champaign measurement than for the Melbourne based studies (owing to the differences in local boundary layer thickness at the location of the experiment). Figure 6 shows how the lower momentum fluid has been gathered over the converging region and ejected away from the wall. It seems like the converging region causes

a pronounced upwelling of the low-speed fluid. The interesting thing is that the weak roll-modes that appear in the mean in-plane velocities (also by Nugroho *et al.* [8]) are not always apparent in the instantaneous flow fields. The first possible scenario is that due to its very weak magnitude ($\lesssim 2\% \ U_\infty$) this mean motion is simply swamped by the instantaneous turbulence. The other possibility is that these violent events happen intermittently with a multitude of length scales and frequencies such that the roll-modes only exist in a time-averaged sense, and are in-fact an artefact of a more violent turbulent process. Further investigation such as conditional analysis on this bursting event is necessary to support this hypothesis.

Conclusions

The behaviour of a turbulent boundary layer under the influence of complex three-dimensional secondary flows generated by herring-bone type riblet surfaces is investigated. Non-simultaneous PIV experiments were conducted in all orthogonal planes of the boundary layer. The large field-of-view cap-
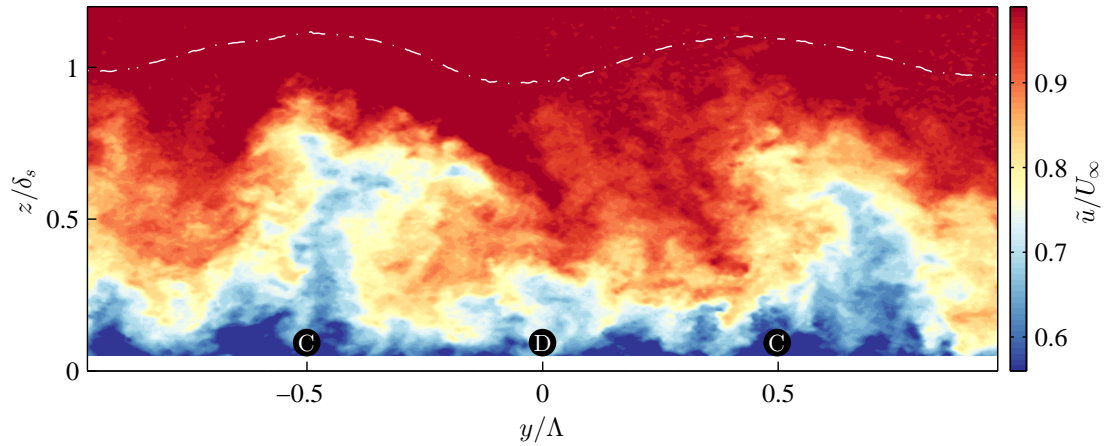
Figure 6: Representative cross-plane view of instantaneous streamwise velocity fields normalised by the freestream velocity $\tilde{u}/U_\infty$. Dot-dashed line highlights the periodicity in the local boundary layer thickness δ

tured using multiple cameras enable us to fully visualise several characteristic events that happen within this flow. In the wall-parallel view, the streaky structures of the near wall region appear to be gathered over the converging part of the riblets. The collected small structures seem to be ejected away from the wall over the converging region, creating an infinitely long stream of low momentum and high turbulence fluids in the logarithmic region. In the outer layer however, these long features seem to become unstable and exhibit signs of a strong three-dimensional distortion or instability.

This instability in the outer layer can also be inferred from the other orthogonal planes. Streamwise−wall-normal plane measurements suggest that these strong collisions and ejections give rise to strongly intermittent events away from the wall. The cross-plane measurements evidence strong ejection events over the converging region that penetrate the outer layer. These events are unstable in time, and seem to move in the spanwise direction under the influence of strong spanwise velocity fluctuations.

Acknowledgements

References

[1] Coceal, O. and Belcher, S. E., A canopy model of mean winds through urban areas. *Quart. J. R. Met. Soc.*, **130**, 2004, 1349-1372.

[2] Hutchins, N. and Marusic, I., Evidence of very long meandering features in the logarithmic region of turbulent boundary layers, *J. Fluid Mech.*, **579**, 2007, 1–28.

[3] Kim, K.C. and Adrian, R.J., Very large-scale motion in the outer layer, *Phys. of Fluids*, **11**, 1999, 417–422.

[4] Mathis, R., Hutchins, N., Marusic, I., Large-scale amplitude modulation of the small-scale structures in turbulent boundary layers, *J. Fluid Mech.*, **628**, 2009, 311–337

[5] Monty, J.P., Stewart, J.A., Williams, R.C. and Chong, M.S., Large-scale scale features in turbulent pipe and channel flows, *J. Fluid Mech.*, **589**, 2007, 147–156

[6] Na, Y., Hanratty, T.J. and Liu, Z., The use of DNS to define stress producing events for turbulent flow over a smooth wall, *Flow Turbul. Combust.*, **66**, 2001, 495–512.

[7] Nugroho, B., Hutchins, N. and Monty, J.P., Large-scale spanwise periodicity in a turbulent boundary layer induced by highly ordered and directional surface roughness, *Int. J. Heat Fluid Flow*, **41**, 2013, 90–102.

[8] Nugroho, B., Gnanamanickam, E.P., Kevin, Monty, J.P. and Hutchins, N., Roll-modes generated in turbulent boundary layers with passive surface modification, in *AIAA*, 52, 2014.

[9] Raupach, M.R., and Antonia, R.A. and Rajagopalan, S., Rough-wall turbulent boundary layers, *Appl. Mech. Rev.*, **44**, 1991, 1–25.

[10] de Silva, C.M., Gnanamanickam, E.P., Atkinson, C., Buchman, N.A., Hutchins, N., Soria, J., Marusic, I., High spatial range velocity measurements in a high Reynolds number turbulent boundary layers, *Phys. of Fluids*, **26**, 2014, 025117.

[11] Soloff, S.M., Adrian, R.J. and Liu, Z.-C., Distortion compensation for generalized stereoscopic particle image velocimetry, *Meas. Sci. Technol.*, **8**, 1997, 1441–1454.

[12] Wu, Y. and Christensen, K.T., Spatial structure of a turbulent boundary layer with irregular surface roughness, *J. Fluid Mech.*, **655**, 2010, 380–418.